COBEM 2023 27TH INTERNATIONAL CONGRESS OF MECHANICAL ENGINEERING

ABCM Brazilian Society of Mechanical Sciences and Engineering
27th ABCM International Congress of Mechanical Engineering
December 04-08, 2023, Florianópolis-SC, Brazil

COB-2023-2071
UNSTEADY AERODYNAMIC ANALYSIS OF AN EMULATED WANDERING ALBATROSS

Lucas Ribeiro Alves
Ricardo Luiz Utsch de Freitas Pinto
Oscar Ricardo Sandoval Rodriguez
Department of Mechanical Engineering, Federal University of Minas Gerais, Av. Antônio Carlos, Belo Horizonte, 31270-901, Minas Gerais, Brazil
lucasralves@ufmg.br
utsch@demec.ufmg.br
oscar@demec.ufmg.br

Abstract. *This paper presents an unsteady aerodynamic study of the Wandering Albatross bird (Diomedea Exulans) in order to explain how the flapping motion is able to keep flight in balance and what are some limiting factors involved. The aerodynamic modeling of the wing applies a strip theory model, in which the wing is discretized into sections through which the distributed forces are calculated. The aerodynamic model also accounts for non-stationary effects such as dynamic stall and the Knoller-Betz effect. The analysis indicates that the flight speed has biological and aerodynamic limiting factors. The biological limit is an upper limit and is caused by the increase in power required to perform the movement exceeding the power available through the musculature. The aerodynamic factor is the lower limit and is caused by the increase in stalled regions on the wing as flight speed decreases. The analysis applied in this work can be extended to other bird species.*

Keywords: *unsteady aerodynamics, flapping motion, dynamic stall, Knoller-Betz effect, and wandering albatross.*

1. INTRODUCTION

The bird's flight has intrigued humanity for centuries. In the XVI century, Leonardo da Vinci produced the *Codex on the Flight of Birds*, in which he investigated the bird's flights and idealized flight machines (SNASM, 2013a). Three hundred years later, in the late XIX century, Otto Lilienthal created the first machine heaviest than air capable of soaring (SNASM, 2013b). A decade later, the Wright Brothers (1903) and Santos Dumont (1906) built, separately, the first airplanes (Klein, 2016).

The birds are capable of flying in different ways, by beating their wings while moving in space, soaring, or remaining still in the air while the wings are beating like a hummingbird. In this paper, the analyzed flight, in which the wing is beating and enough thrust and lift are produced to counterbalance the drag and weight respectively, the bird's horizontal velocity and altitude oscillate around a constant value during one wing beat as shown in Figure 1. During this type of flight, the wing-beat frequency remains approximately constant and other flight parameters have to adjust for each flight velocity (Kardong, 2011).

Figure 1. Representation of a bird's altitude oscillating around a constant value.

The wing beat motion may be split into the descending and ascending phases. The flight feathers (Figure 2) present on the bird's wings and tail are asymmetrical and behave differently in these phases. During the ascending phase, the asymmetry causes a rotation as shown in Figure 2, which enables the passage of air between the feathers. Therefore, less aerodynamic force is created contrary to the wing movement. On the other hand, during the descending phase, the contact between the feathers prevents them from rotating (Shyy *et al.*, 2008).

A characteristic of a bird's wings is the Alula, shown in Figure 3, which corresponds to the bird's thumb. It can be seen in the leading edge of modern birds and works as slats in airplanes, increasing the stall angle during high angle of attack (Kardong, 2011).

During the analysis of non-stationary aerodynamics, two essential characteristics must be considered: dynamic stall and the Knoller-Betz effect. Dynamic stall refers to a delay in stall experienced by airfoils during unsteady motion (Carr,

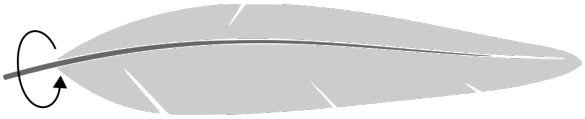

Figure 2. Application of rotation in a hypothetical flight feather.

1988). In this paper, the dynamic stall is treated as an increase in the stall angle of each section of the wing shown in Figure 8. The increase depends on, among other factors, the local change in attack angle over time. On the other hand, the Knoller-Betz effect relates to the appearance of a thrust force, particularly observed in flapping wings. This phenomenon arises due to the resulting velocity in each section of the wing, which, due to the beating movement, produce lift in the opposite direction to the free flow velocity (Jones *et al.*, 1998).

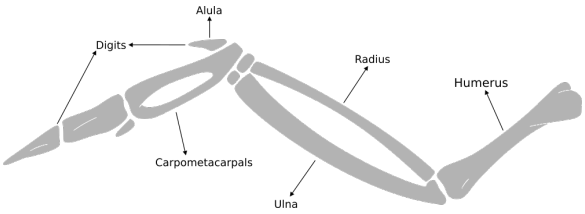

Figure 3. Wing bone structure.

This paper aims to explain how some flight parameters, such as frequency beat, wing beat amplitude, and airspeed affect the bird's flight. To do so, an approximate model of a Wandering Albatross wing is developed, and it's applied an aerodynamic model that takes into account the unsteady motion, such as dynamic stall, and the knoller-Betz effect (DeLaurier, 1993). An investigation is made to discover the factors that limit flight speed in equilibrium while the wing is beating.

2. METHODOLOGY

The analysis is made in 4 parts, described as: i) Definition of the geometric parameters necessary to describe the wing and body; ii) The determination of the airfoils of the wing sections, based on the Reynolds Number calculated considering the flight speed limits; iii) The calculus of the flight speed limits, based on the Strouhal number; iv) The aerodynamic model to calculate the forces in each section of the wing.

In order to estimate all the parameters defined in the methodology, previous works, images, and videos are considered. Aiming to fulfill the requirements, additional hypotheses and models are formulated to complete these three means.

2.1 Geometry

The bird's geometry, Figure 4, is represented by a parametric model, where all dimensions are normalized with respect to the wingspan. This geometric model, essential for describing the wing, central body, and tail, approximates the bird's body as a revolution of a parabolic profile. Its definition serves to calculate a feasible drag, enabling a comparison with the thrust produced by the wings.

In accordance with Wei *et al.* (2013), the wingspan (b) can be approximated as a function of the bird's mass (m) for various bird species using Equation 1.

$$b = 1.704 m^{\frac{1}{3}} \tag{1}$$

The Table 1 presents the normalized and real values of the parameters presented in Figure 4, considering a bird mass of 7kg, which falls within the weight range of adult species (OCEANWIDE, 2020), and a wingspan of 3.26 meters, obtained from Equation 1.

Table 1. Bird's normalized parameters and its values.

Parameter	$\mathbf{c_1}$	$\mathbf{c_2}$	$\mathbf{c_3}$	$\mathbf{a_1}$	$\mathbf{a_2}$	$\mathbf{a_3}$	$\mathbf{l_1}$	$\mathbf{l_2}$	$\mathbf{l_2}$	$\mathbf{r_1}$	$\mathbf{r_2}$	$\mathbf{r_3}$
Normalized	0.142	0.095	0.095	0.151	0.151	0.189	0.318	0.037	0.019	0.085	0.063	0.072
Value [m]	0.493	0.493	0.616	0.463	0.155	0.155	1.037	0.121	0.062	0.277	0.205	0.235

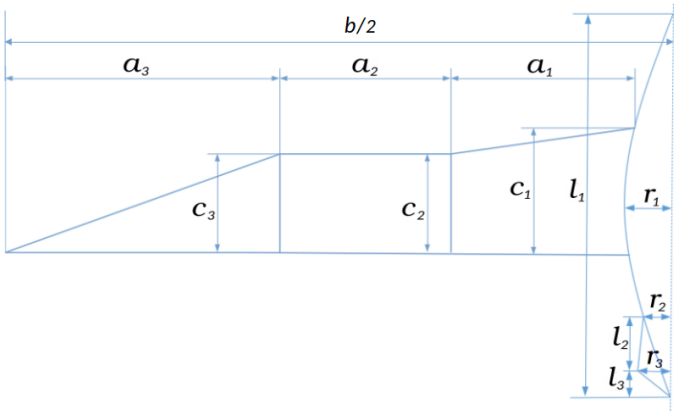

Figure 4. Geometric model.

2.2 Wing Airfoils

In order to define the wing's airfoils, the physical characteristics of birds and the expected aerodynamic properties are considered. Birds have wings with aerodynamic profiles that exhibit greater camber and relative thickness at the root to display the desired aerodynamic characteristics and to accommodate the skeletal and muscular structure of the region (Kardong, 2011). The more pronounced camber increases the lift coefficient of the region, but it may lead to a reduction in the stall angle, which is an important factor to consider, as the wing's motion induces a relative velocity to the profile, causing more significant variations in the angle of attack at the wingtip (Anderson, 2001). As the wing extends towards the tip, the thickness of the profiles decreases, eventually consisting solely of feathers at the ends (Kardong, 2011).

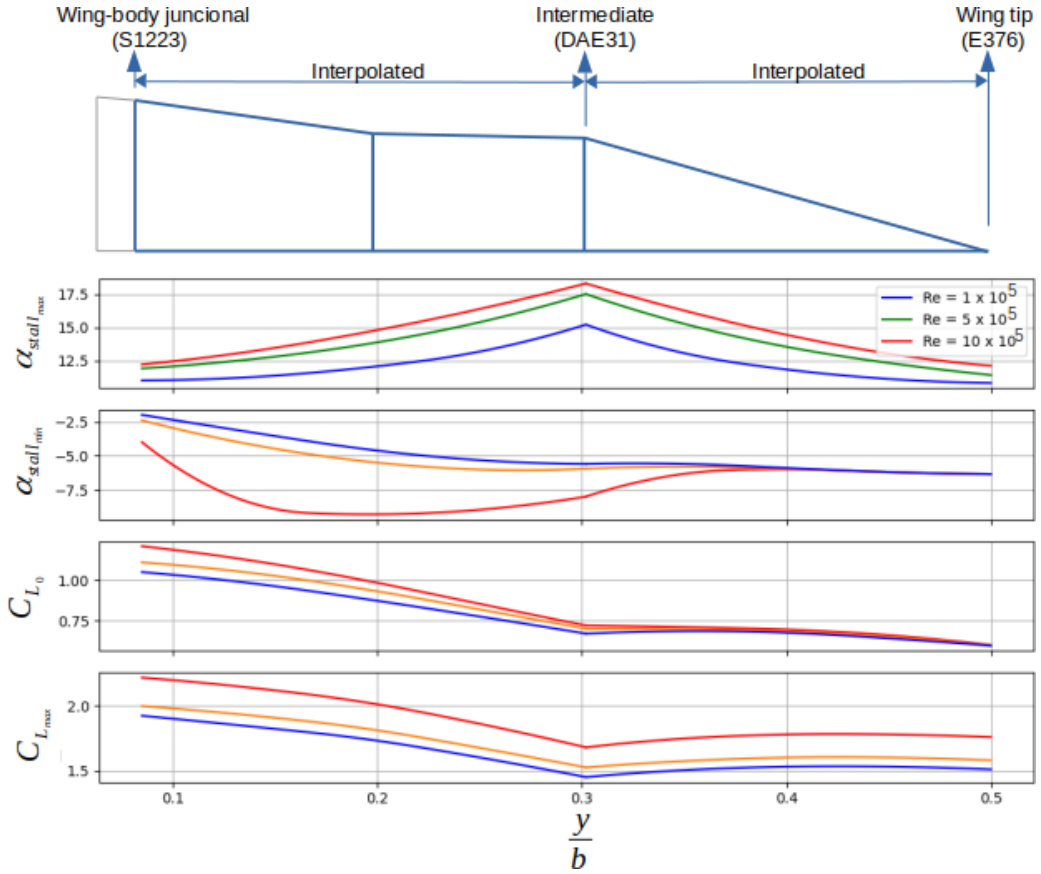

Figure 5. Aerodynamic parameters distribution over the semispan.

An important consideration that simplifies the analysis of the motion of the wing is that the joint that connects the humerus to the radius/ulna is considered rigid. Thus, for practical purpose, the first and second sections ($y < a_1 + a_2$),

shown in Figure 4, can be treated as a single part since they don't have relative motion in relation to each other.

With this in mind, 3 profiles are defined: 1) the S1223 at the wing-body junction; 2) the DAE31 between the second and third section (intermediate section); 3) the E376 at the wing tip. In order to calculate the aerodynamic characteristic of the wing, new profiles were interpolated between the three previously defined. Then a curve fit was made in the aerodynamic parameters $C_{L_{max}}$, C_{L_0}, $\alpha_{stall_{min}}$ and $\alpha_{stall_{max}}$ calculated by the software XFLR5 and they are presented in Figure 5, distributed over the normalized span.

2.3 Flight speed

The Stroudal number, Equation 2, is the ratio between the inertial forces due to local acceleration and convective acceleration and assumes values between 0.2 and 0.4 for birds during cruise flight (Shyy *et al.*, 2008). The f, L and U are the wing beat frequency, the characteristic length of the vortexes caused by the wing motion and the freestream velocity respectively. Therefore, the parameter U is defined in order to keep S_t between its bounds.

$$S_t = \frac{fL}{U} \tag{2}$$

The wing-beat frequency, considered to be constant during the equilibrium flight, is estimated as in Equation 3, based on bird's mass m and wing area S (Wei *et al.*, 2013).

$$f = 3.38\, m^{\frac{3}{8}} b^{-\frac{23}{24}} S^{-\frac{1}{3}} \;\approx\; 2.1Hz \tag{3}$$

The characteristic length (L) of the vortexes caused by the wing motion is approximated as the vertical displacement of the wing tip during a wing beat cycle. Aiming to calculate the length L, the angles β, δ, γ, ϕ, ρ and σ are defined as shown in Figure 6. The angle β can be understood as the pitch angle applied at the wing root, which causes the wing to rotate about the $\hat{y}$ axis. In order to simplify the analyses, the angles ϕ, ρ and σ will be defined as zero and the angles β, δ and γ will be defined as functions of time.

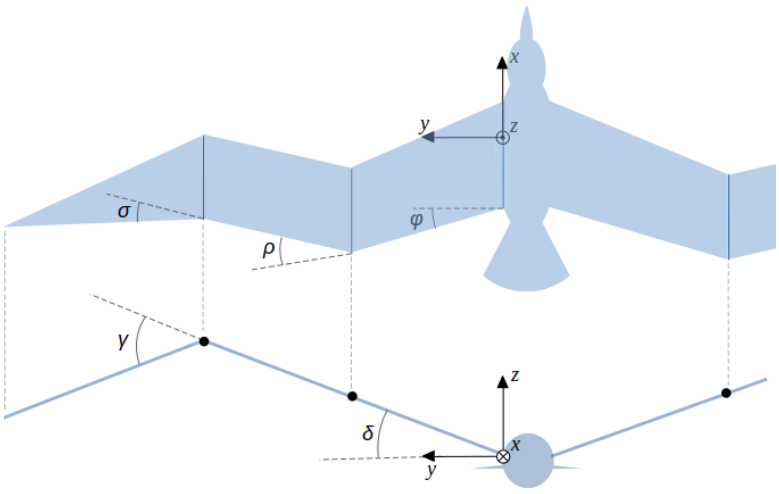

Figure 6. Angles description using a top and front view of the bird.

As the wing-beat frequency remains approximately constant in a wide range of velocity (Wei *et al.*, 2013), other parameters vary to generate the necessary forces to maintain equilibrium flight. Therefore, as the wing-beat frequency is already defined, the motion of the first two segments and the third segment of the wing were estimated based on a video analysis of a Wandering Albatross during flight.

Hence, it is possible to approximate the angles δ and γ as periodic functions of time, with 15^o of amplitude as the reference value for both angles. The angle β could not be determined by the videos or searching in the bibliography, it was only found that birds can change this angle during flight (Kardong, 2011). During the video analysis, was noticed that the wing passes slightly below the horizontal during the descending phase and this angle was defined as 10^o. The periodic functions for the angles δ, β and γ can be seen in the Figure 7, where the subscript A represents the amplitude and B the displacement in relation to the origin.

Therefore, based on the definition of $\delta(t)$, $\beta(t)$ and $\gamma(t)$, the characteristic length, L is calculated approximately as $0.7m$ and, considering the limits of 0.2 and 0.4 for the Stroudal number in Equation 2, the flight velocity is between, approximately, 9 and 18 m/s.

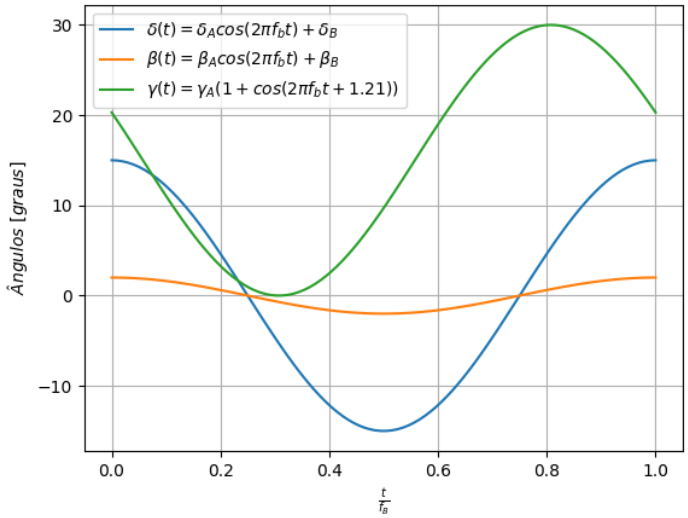

Figure 7. Angles δ, β and γ as function of time during one wing-beat.

2.4 Wing

A modified strip theory was chosen to calculate the wing forces (DeLaurier, 1993). As shown in Figure 8, there are four forces acting on the wing section, two parallel to the chord, dT_s and dR, and two forces perpendicular to the chord, dN_c and dN_a. The forces account for steady effects, as the normal force due to the instantaneous circulation (N_c) and the viscous and pressure drag (R), and unsteady effects, as the thrust due to transition of the suction peak between the upper and lower surface (T_s), and the normal force due to change in circulation in time (N_a)[1]. The calculation of the forces is not explained in detail in this Section. Thus, verify reference (DeLaurier, 1993) for more details.

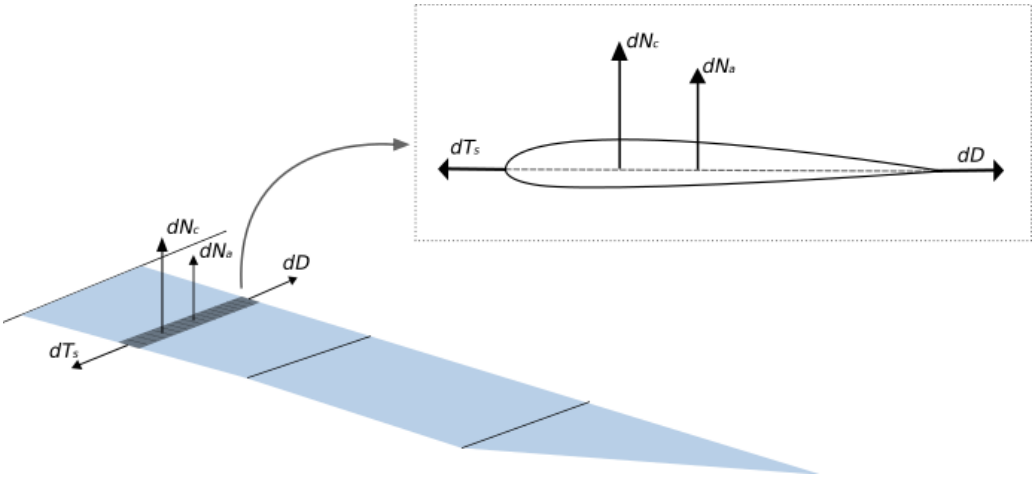

Figure 8. Wing section parameters.

Therefore, considering the angles $\delta(t)$, $\beta(t)$ and $\gamma(t)$ previously defined, the lift (L) and thrust (T) can be calculated by Equations 4 and 5.

$$L(t) = L_N(t) + L_C(t) \tag{4}$$

$$T(t) = T_N(t) + T_C(t) \tag{5}$$

Where,

[1] All forces are calculated considering the aerodynamic parameters described in Subsection 2.2 (Wing Airfoils).

$$L_N(t) = 2 \int_0^{a_1+a_2+a_3} \left(\lambda sin\big(\delta(t)\big) sin\big(\gamma(t)\big) + cos\big(\delta(t)\big) cos\big(\beta(t)\big)\big(1 - \lambda + \lambda cos\big(\gamma(t)\big)\big)\right) (dN_a + dN_c) \tag{6}$$

$$L_C(t) = 2 \int_0^{a_1+a_2+a_3} \left(cos\big(\delta(t)\big) sin\big(\beta(t)\big)\right) (dT_s - dR) \tag{7}$$

$$T_N(t) = 2 \int_0^{a_1+a_2+a_3} -sin\big(\beta(t)\big) cos\big(\gamma(t)\lambda\big) (dN_a + dN_c) \tag{8}$$

$$T_C(t) = 2 \int_0^{a_1+a_2+a_3} cos\big(\beta(t)\big) (dT_s - dR) \tag{9}$$

$$\lambda = \begin{cases} 1, & \text{if } y \geq a_1 + a_2 \\ 0, & \text{otherwise} \end{cases} \tag{10}$$

2.5 Body

The thrust generated by the wing must overcome the drag. Based on (Barrowman, 1967), the pressure and viscous drag were calculated separated, and then, added. The viscous drag is considered independent of the Reynolds number due to the surface roughness caused by the fathers. Therefore, the total drag coefficient, calculated considering a Mach Number of 0.02, is 0.144, using the thicker section of the body as the reference area.

2.6 Dynamic Stall Analysis

The increase in stall angle due to wing motion, known as dynamic stall, can be calculated by Equation 11, considering that the flow abruptly detaches from the surface starting from the leading edge, (Zakaria, 2016). In this scenario, after the increased linear region of the lift coefficient, the forces in the chord direction shown in Equations 4 and 5 are neglected and the forces acting in the normal direction are replaced by $(N_c)_{sep}$ and $(N_a)_{sep}$, also presented in reference (DeLaurier, 1993).

$$\Delta\alpha(y,t) = 0.51 \left(\frac{\frac{\partial\alpha}{\partial t}(y,t)}{\left|\frac{\partial\alpha}{\partial t}(y,t)\right|}\right) \sqrt{\left(\frac{c(y)\left|\frac{\partial\alpha}{\partial t}(y,t)\right|}{2U}\right)} \tag{11}$$

2.7 Numerical Approximation

As stated by Equation 12 and 13, Equations 4 and 5 are approximate as the sum of contributions of the n_y wing sections, by considering the differentials, for example dN as ΔN, a force at a discrete region on the wing. The subscripts N and C represent the normal and chord component respectively.

$$L(t) = 2\sum_{i=1}^{n_y} (\Delta L_{N_i} + \Delta L_{C_i}) \tag{12}$$

$$T(t) = 2\sum_{i=1}^{n_y} (\Delta T_{N_i} + \Delta T_{C_i}) \tag{13}$$

Where:

$$\Delta L_N = \big(\lambda_i sin\big(\delta(t)\big) sin\big(\gamma(t)\big) + cos\big(\delta(t)\big) cos\big(\beta(t)\big)\big(1 - \lambda_i + \lambda_i cos\big(\gamma(t)\big)\big)\big)\left(\Delta N_{a_i} + \Delta N_{c_i}\right) \tag{14}$$

$$\Delta L_C = \big(cos\big(\delta(t)\big) sin\big(\beta(t)\big)\big)\left(\Delta T_{s_i} - \Delta R_i\right) \tag{15}$$

$$\Delta T_N = -sin\big(\beta(t)\big) cos\big(\gamma(t)\lambda_i\big)\left(\Delta N_{a_i} + \Delta N_{c_i}\right) \tag{16}$$

$$\Delta T_C = cos\big(\beta(t)\big)\left(\Delta T_{s_i} - \Delta R_i\right) \tag{17}$$

2.8 Power Generated by the Pectoral Muscle

The pectoral muscle is the largest muscle in birds and it is the dominant muscle for the descent phase of the wing beat. To calculate the power necessary in the descent phase, the change in mechanical energy of each section of the wing is calculated and then added, considering the mass in each section proportional to the local chord.

The wing mass, M_w, as function of the total mass, M, calculated based on Equation 18 is 1.2kg, (Berg and Rayner, 1995), 17% of the total mass and, according to (Kardong, 2011), the maximum available power for this amount of muscle is about 180,0W.

$$M_w = 0.1412 M^{1.098} \tag{18}$$

3. RESULTS AND DISCUSSION

3.1 Distributed Force

In order to analyze the force distribution over the wing, a simulation was made considering a velocity flight of 10.0 m/s and the angles $\delta(t), \beta(t)$ and $\gamma(t)$ in Equations 19, 20 and 21. The value of $\beta = 0.31^o$ generates a lift equal to the birds weight.

$$\delta(t) = 15 cos\left(t\frac{2\pi}{T}\right) + 10.0 \tag{19}$$

$$\beta = 0.31 \tag{20}$$

$$\gamma(t) = 15\left(1 + cos\left(t\frac{2\pi}{T} + 1.21\right)\right) \tag{21}$$

The Figure 9a shows that lift has a sinusoidal shape over time and that thrust is produced predominantly in the downstroke, being negative practically the rest of the time. Figure 9b analyzes the distribution of lift and thrust along the span during the downstroke of the wing, shown in Figure 9a. It is possible to notice that the first two sections are responsible for generate lift, about 77.6% of total lift, and the third section, thrust, about 82.8% of total thrust, considering only this instant. In addition, the thrust close to the body has negative values, indicating that drag, in this region, is greater than the propulsive force.

3.2 Integrated Force

Intending to analyze the effect of the forces on the wing during a wing-beat, Equations 12 and 13 were used to calculate the integrated forces over the wing, as shown in Figure 9a. The propulsive and lift forces are collinear and perpendicular to the free flow, respectively, with the propulsive force being positive when opposed to the flow.

A peak can be seen in both lift and propulsive forces during the descending phase, as expected. The lift force has a sinusoidal shape, however, during the ascending phase, there are factors that were not considered in the model, such as the rotation of the feathers on the wing tip, which can modify the presented force. The same occurs for the propulsive force that has a positive value in the ascending phase, which, due to the implemented model, may not agree with the reality.

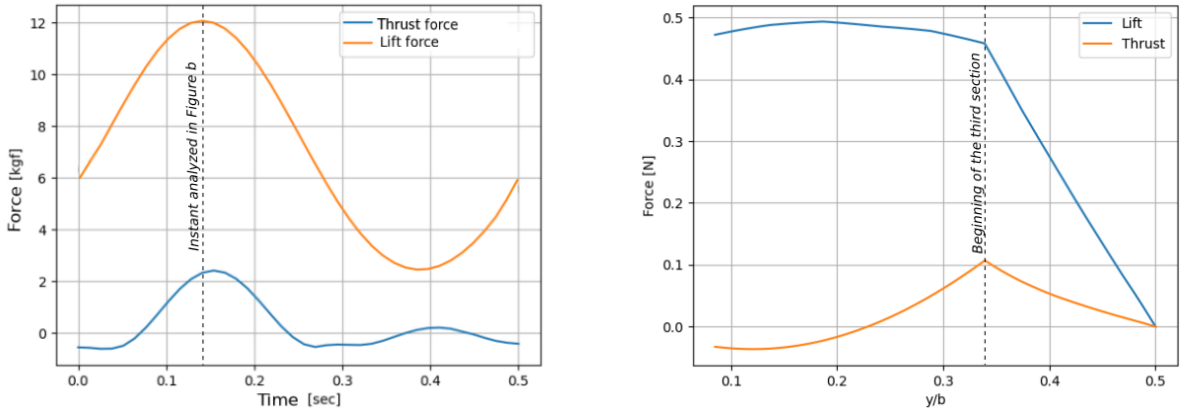

(a) Thrust and lift force during a wing beat.

(b) Distributed thrust and lift during the downstroke.

Figure 9. Distributed force during a wing beat and in the middle of downstroke.

3.3 Stalled Regions

The study of stalled regions was made by analyzing how it is affected by the angle $\beta(t)$. First, the value of β_B was defined so that the wing had stalled regions during 10% of a wing-beat. Then, the value of β_A, that represents the amplitude, was increased and, as can be seen in Figure 10, it was possible to eliminate all stalled regions of the wing during a wing-beat. However, despite a small increase in the total force for small values of β_A due to the reduction of stalled regions, the force decreases for larger values of β_A, as a result of the reduction of the relative angle of attack in each section. Therefore, the angle $\beta(t)$ may play an important role in wing stall dynamics, but further analysis, with a more accurate model, is necessary to understand how the angle $\beta(t)$ act during a wing-beat.

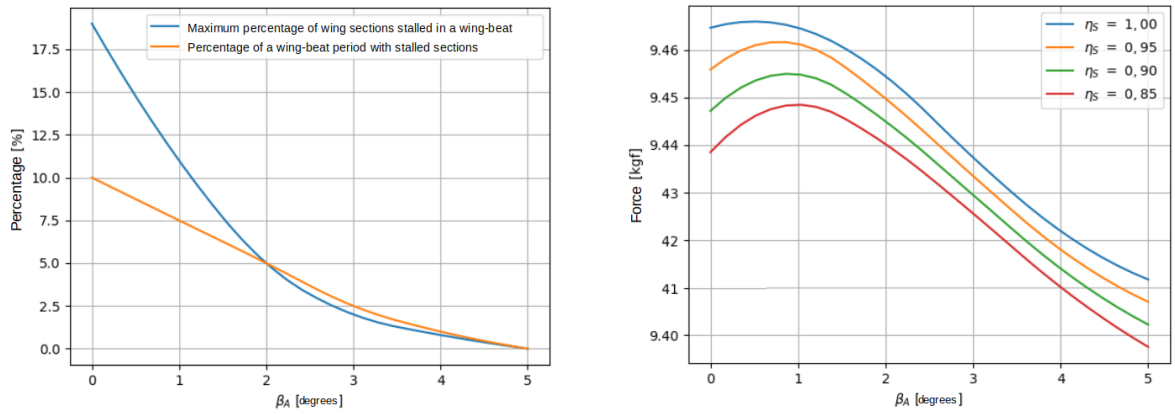

(a) Stalled sections.

(b) Total force.

Figure 10. Percentage of a wing-beat period with stalled sections and total force as a function of β_A

3.4 Flight Limiting Factors

In order to verify the flight speed limiting factors, the values of δ_A, γ_A and β_B necessary to maintain equilibrium flight were analyzed as function of flight speed, Figure 11. The parameters were calculated until a velocity of 12 m/s due to the increase in power required to perform the movement, shown in Figure 12, which exceeded the maximum value predicted. The lower limit occurred because it was not possible to find values for the parameters that would generate an equilibrium flight, due to the first two sections of the wing that started to stall and is responsible for most of the lift generated by the wing.

Figure 12, as already mentioned, shows the maximum power required to perform the movement. As expected, the maximum value was reached during the downstroke phase, in which there is a peak in lift and thrust. The value found for the maximum available power of 180.0W is reached at around 12.0 m/s, representing a biological limit for the bird's speed, based on the conditions considered.

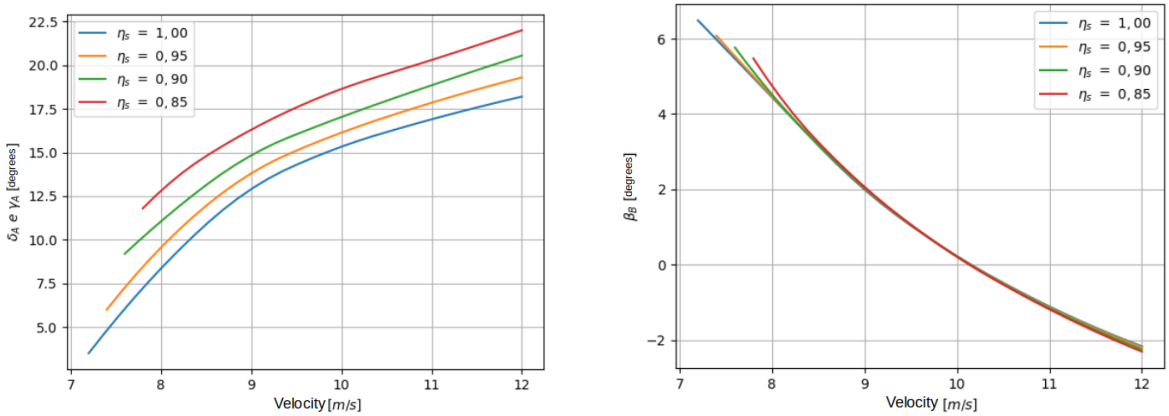

(a) Angles δ_A and γ_A. (b) Angle β_B.

Figure 11. Angles δ_A, γ_A and β_B necessary to maintain equilibrium as function of velocity flight.

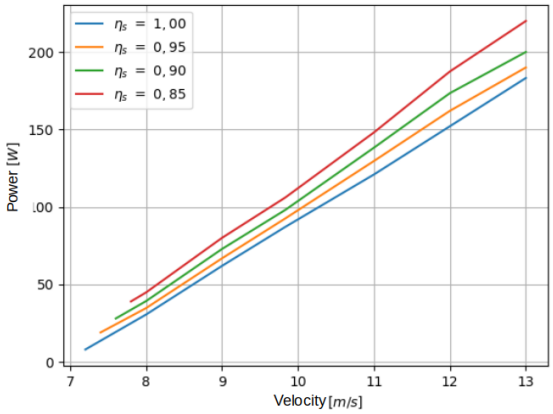

Figure 12. Maximum power is necessary to execute the flapping movement.

4. CONCLUSION

The distribution of the forces on the wing during the downstroke showed that the lift force is generated predominantly by the first two sections of the wing, close to the root, and the thrust in the third section, close to the tip.

In addition, the analysis showed that small values of β_A are sufficient to reduce the number of stalled regions (for example, 38% for $\beta_A = 1.0^o$). However, the increase in the range of $\beta(t)$ resulted in a decrease of the resulting force, impacting more significantly on the propulsive force, that reached negative values for β_A greater than 2.5 degrees.

Two limiting factors in flight speed were found in the analysis, one of aerodynamic nature and the other of biological nature. The aerodynamic factor is a lower bound, caused by an increase of stalled sections of the wing, mainly of the first two sections, in which most of the lift is generated. The biological factor is an upper bound, caused by the power capable of being generated by the pectoral muscle, which reached the maximum value for a velocity of about 12.0m/s.

5. ACKNOWLEDGEMENTS

The authors thank the support of the Coordenação de Aperfeiçoamento de Pessoal de Nível Superior (CAPES) for the scholarship awarded during this project.

6. REFERENCES

Anderson, J.D., 2001. *Fundamentals of Aerodynamics*. McGraw-Hill, New York.

Barrowman, J.S., 1967. "The practical calculation of the aerodynamic characteristics of slender finned vehicles". https://ntrs.nasa.gov/api/citations/20010047838/downloads/20010047838.pdfs. Accessed 23 Nov 2020.

Berg, C.V.D. and Rayner, J.M.V., 1995. "The moment of inertial of bird wings and the inertial power requirement for flapping flight". *The Journal of Experimental Biology*, Vol. 198, pp. 1655–1664.

Carr, L.W., 1988. "Progress in analysis and prediction of dynamic stall". *Journal of Aircraft*, Vol. 25, pp. 6–17.

DeLaurier, J.D., 1993. "An aerodynamic model for flapping-wing flight". *The Aeronautical Journal of the Royal Aeronautical Society*, Vol. 97, p. 125–130.

Jones, K.D., Dohring, C.M. and Platzer, M.F., 1998. "Experimental and computational investigation of the knoller-betz effect". *AIAA Journal*, Vol. 36, No. 7, pp. 1240–1246. doi:10.2514/2.505. URL `https://doi.org/10.2514/2.505`.

Kardong, K.V., 2011. *Vertebrados, Anatomia Comparada, Função e Evolução*. Roca, São Paulo.

Klein, C., 2016. "History faceoff: Who was first in flight?" https://www.history.com/news/history-faceoff-who-was-first-in-flight. Accessed 23 Nov 2020.

OCEANWIDE, 2020. "Wandering albatross". https://oceanwide-expeditions.com/to-do/wildlife/wandering-albatross. Accessed 23 Nov 2020.

Shyy, W., Lian, Y., Tang, J., Viieru, D. and Liu, H., 2008. *Aerodynamics of Reynolds Number Flyers*. Cambridge University Press, Cambridge.

SNASM, 2013a. "Leonardo da vinci's codex on the flight of birds". Smithsonian National Air and Space Museum, https://airandspace.si.edu/exhibitions/codex/. Accessed 23 Nov 2020.

SNASM, 2013b. "Lilienthal glider". Smithsonian National Air and Space Museum, https://airandspace.si.edu/collection-objects/lilienthal-glider/nasm$_A$19060001000.$Accessed23Nov2020$.

Wei, S., Hikaru, A., Chang-Kwon, K. and Hao, L., 2013. *An Introduction to Flapping Wing Aerodynamics*. Cambridge University Press, Cambridge.

Zakaria, M.Y., 2016. *Unsteady Nonlinear Aerodynamic Modeling and Applications*. Ph.D. thesis, Virginia Polytechnic Institute and State University, Blacksburg, Virginia.

7. RESPONSIBILITY NOTICE

The authors are solely responsible for the printed material included in this paper.